δ-COP modulates Aβ peptide formation via retrograde trafficking of APP

Karima Bettayeb[a], Jerry C. Chang[a], Wenjie Luo[a,1], Suvekshya Aryal[a], Dante Varotsis[a], Lisa Randolph[a], William J. Netzer[a], Paul Greengard[a,2], and Marc Flajolet[a,2]

[a]Laboratory of Molecular and Cellular Neuroscience, The Rockefeller University, New York, NY 10065

Contributed by Paul Greengard, March 14, 2016 (sent for review December 15, 2015; reviewed by David M. Holtzman and Bradley T. Hyman)

The components involved in cellular trafficking and protein recycling machinery that have been associated with increased Alzheimer's disease (AD) risk belong to the late secretory compartments for the most part. Here, we hypothesize that these late unavoidable events might be the consequence of earlier complications occurring while amyloid precursor protein (APP) is trafficking through the early secretory pathway. We investigated the relevance to AD of coat protein complex I (COPI)-dependent trafficking, an early step in Golgi-to-endoplasmic reticulum (ER) retrograde transport and one of the very first trafficking steps. Using a complex set of imaging technologies, including inverse fluorescence recovery after photobleaching (iFRAP) and photoactivatable probes, coupled to biochemical experiments, we show that COPI subunit δ (δ-COP) affects the biology of APP, including its subcellular localization and cell surface expression, its trafficking, and its metabolism. These findings demonstrate the crucial role of δ-COP in APP metabolism and, consequently, the generation of amyloid-β (Aβ) peptide, providing previously nondescribed mechanistic explanations of the underlying events.

amyloid | COPI | retrograde transport | Alzheimer | trafficking

Alzheimer's disease (AD) is a complex pathological condition that involves various subcellular compartments and organelles, and affects a range of biological processes, such as protein maturation, mitochondrial function, autophagy, and protein trafficking (1–5).

One of its hallmarks is the presence of amyloid plaques composed of aggregated amyloid-β (Aβ) peptides that result from the sequential cleavage of the amyloid precursor protein (APP) (1). APP is initially cleaved by beta-secretase (BACE1), producing secreted sAPPbeta and intracellular APP-beta–C-terminal fragment (APP-beta-CTF) (6). APP-beta-CTF is then cleaved by the tetrameric protein complex called γ-secretase to release Aβ peptides (7). Those proteolytic cleavages occur concomitantly with APP trafficking, mainly from the plasma membrane to late endosomes (1, 8). However, little attention has been given to how APP processing might be affected by its trajectory through the early secretory pathway involving the coatomer protein complexes that regulate retrograde [Golgi-to-endoplasmic reticulum (ER)] and anterograde (ER-to-Golgi) transport along this pathway (9). In particular, the mechanisms that accompany APP maturation and direct it toward the cell surface have been overlooked.

Here, we investigated the relevance of an early trafficking step in APP maturation, involving coat protein complex I (COPI)-dependent trafficking. COPI is a complex of seven subunits that coat vesicles mainly for protein trafficking in the early secretory pathway. This complex is crucial for retrograde transport of proteins from the Golgi apparatus back to the ER, as well as among Golgi compartments (10, 11).

Our results demonstrate that COPI subunit δ (δ-COP) regulates APP intracellular trafficking, controlling its maturation and thus the production of Aβ peptides. Altogether, our findings demonstrate the physiological relevance of δ-COP in AD pathogenesis. Furthermore, whereas AD studies focus mostly on the efficiency and/or accessibility of the proteases involved in APP cleavages, our study suggests that the origin of the problem might be, in fact, directly linked to the nature of APP and occurring far upstream of the processing sites, namely, at the endocytic pathway level.

Results

δ-COP Regulates Aβ Production and Interacts with APP. The COPI complex is responsible for the retrograde Golgi-to-ER transport, and therefore represents an important component of the machinery affecting protein maturation. To investigate the effect of the COPI complex on Aβ peptide generation, we silenced each of the seven subunits of the complex individually using pools of siRNAs in N2a-695 cells at several time points.

Thirty-six hours posttransfection, a successful reduction of expression was achieved for each COPI subunit (Fig. 1*A* and Fig. S1 *A* and *B*). Remarkably only δ-COP silencing significantly decreased Aβ40 production at that time point (Fig. 1*B*). At 48 h posttransfection, three additional COPI subunits (α, β, and β′ subunits) were found to influence Aβ production, but the toxicity resulting from silencing each of these three subunits individually was significant, and led to some degree of cell death (Fig. 1*C*). Only minor or no toxicity was observed at 36 h (Fig. 1*D*). The efficacy of δ-COP silencing on Aβ40 reduction increased with time up to 48 h (61%; Fig. 2*A*); we then used this time point in all subsequent studies. We also found the inverse relationship to be true, where δ-COP overexpression caused an increase in Aβ40 production in N2a-695 cells (Fig. 2*B*). Similar results were obtained on endogenous APP when using N2a cells. The results showed that δ-COP expression controls

Significance

Alzheimer's disease (AD) is characterized by the presence of amyloid plaques resulting from the aggregation of amyloid-β (Aβ) peptides produced via sequential cleavage of amyloid precursor protein (APP). Cleavages happen concomitantly with APP trafficking from the plasma membrane to late endosomes. However, the role of an early trafficking pathway, the coat protein complex I (COPI)-dependent trafficking, has been overlooked. The present study demonstrates that, using a complex set of imaging technologies coupled to biochemical experiments, COPI subunit δ (δ-COP) affects the biology of APP, including its subcellular localization, cell surface expression, and trafficking, as well as its metabolism. Altogether, these findings demonstrate the physiological relevance of δ-COP in AD pathogenesis.

Author contributions: K.B., P.G., and M.F. designed research; K.B., J.C.C., S.A., D.V., L.R., and M.F. performed research; W.L. and W.J.N. contributed new reagents/analytic tools; K.B., J.C.C., W.L., P.G., and M.F. analyzed data; and K.B., J.C.C., W.J.N., P.G., and M.F. wrote the paper.

Reviewers: D.M.H., Washington Univ. School of Medicine; and B.T.H., Massachusetts General Hospital/Harvard Medical School.

The authors declare no conflict of interest.

[1]Present address: Helen and Robert Appel Alzheimer's Disease Research Institute, Brain and Mind Research Institute, Weill Cornell Medical College, New York, NY 10065.

[2]To whom correspondence may be addressed. Email: flajolm@rockefeller.edu or greengard@rockefeller.edu.

This article contains supporting information online at www.pnas.org/lookup/suppl/doi:10.1073/pnas.1604156113/-/DCSupplemental.

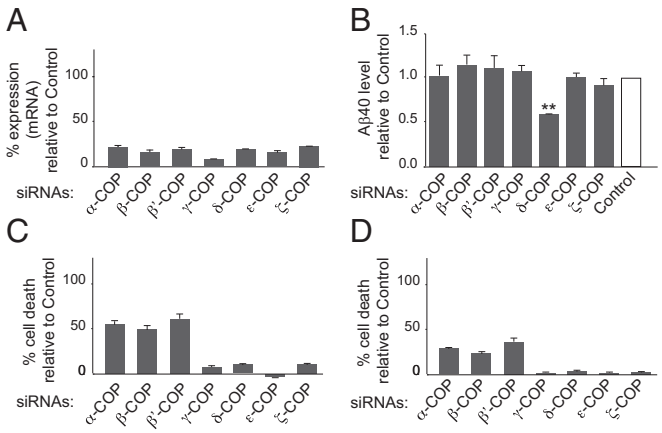

Fig. 1. Effects of COPI subunits on Aβ40 production. (*A*) Analysis of the expression of the seven subunits of the COPI complex by quantitative PCR 36 h posttransfection of N2a-695 cells with siRNA pools for the seven subunits. (*B*) Analysis of Aβ40 level. The results are presented after normalization to the total amount of proteins. Cell death was evaluated by measuring lactate dehydrogenase release 48 h (*C*) or 36 h (*D*) posttransfection using siRNA pools (**$P < 0.01$, two-tailed Student's *t* test; $n = 3$).

Aβ levels and suggested a possible interaction between δ-COP and APP. We confirmed this possibility by demonstrating coimmunoprecipitation of APP and δ-COP (Fig. 2*C*).

δ-COP Silencing Induces APP Accumulation in the Golgi Apparatus and Prevents Its Cell Surface Expression. We next examined the possibility that δ-COP affects Aβ levels by modifying APP trafficking, using sucrose gradients to separate cellular compartments. Silencing δ-COP increased the amount of APP associated with the Golgi by 5.74-fold (Golgi-enriched fraction) and by 1.65-fold in the ER (ER-enriched fraction), whereas total APP increased by 1.4-fold (Fig. 3 *A*–*C*). We also investigated the effect of δ-COP silencing on control actin protein. Depletion of δ-COP had only a mild effect on actin levels (increased 1.33-fold and 1.17-fold in the Golgi and ER, respectively) (Fig. 3 *A* and *B*), indicating that the integrity of the cells was preserved. We reasoned that accumulation of APP in the Golgi apparatus might be compensated for by decreased levels in another subcellular compartment (i.e., the cell surface), which is consistent with the observation that COPI affects cell surface APP levels (12). Using APP biotinylation, we showed that δ-COP silencing dramatically decreased the amount of APP at the cell surface (Fig. 3*D*). Similar results were obtained in N2a cells. The silencing of δ-COP could either prevent APP from reaching the plasma membrane or affect APP endocytosis. To determine whether δ-COP also influences the kinetics of APP endocytosis, cell surface proteins were biotinylated and their internalization was assessed over time. Compared with control siRNA, the kinetics of APP endocytosis remained unchanged after reducing δ-COP (Fig. 3*E*).

APP Maturation Is Affected by δ-COP Silencing. We next tested whether δ-COP silencing affects maturation of APP. Mature and immature APP isoforms were resolved by immunoblot (Fig. 4*A*). Lowering δ-COP with siRNA reduced the relative levels of mature APP in a time-dependent manner (decrease of 67.8% ± 1.52 at 36 h and 76.3% ± 1.2 at 48 h), whereas Brefeldin A (BFA), a drug that disrupts the Golgi apparatus, eliminated the mature APP (Fig. 4*A*). Because δ-COP silencing affects APP maturation, we next investigated which posttranslational modifications (PTMs) δ-COP modulated. We designed six APP mutants lacking different known sites of PTM (13–17) (Fig. 4*B*). Compared with APP-WT, APP lacking known sites for N-glycosylation or palmitoylation produced less Aβ40 (Fig. 4*C*). Interestingly, APP lacking N-glycosylation sites partially failed to respond to δ-COP silencing with respect to Aβ40 (Fig. 4*D*). This observation suggests that COPI could affect Aβ production through a pathway involving N-glycosylation of APP. The δ-COP–mediated change in APP localization and/or deficiency in its maturation might affect APP proteolytic processing. We therefore investigated the possible effect of δ-COP depletion on the α-, β-, and γ-secretase cleavages of APP. Cells were transfected with δ-COP siRNA, and the levels of secreted sAPPbeta and sAPPalpha (cleavage products of the β- and α-secretase, respectively) were measured. Reducing δ-COP levels decreased the APP proteolytic product sAPPbeta at 36 and 48 h, whereas sAPPalpha remained unchanged (Fig. 4 *E*–*G*). In this cellular system, the amount of cognate APP fragment APP-beta-CTF is undetectable. Reduction of δ-COP in N2a cells transfected with APP-beta-CTF, the substrate of γ-secretase, also significantly reduced Aβ40 production (Fig. 4*H*), whereas APP-beta-CTF is unchanged in this system (Fig. 4*H*, *Lower*). These findings demonstrate that δ-COP affects multiple steps of APP proteolytic processing in the amyloidogenic pathway.

δ-COP Silencing Perturbs Dynamic Trafficking of APP in the Early Secretory Pathway. To assess the subcellular distribution of APP and δ-COP further, an optimized confocal imaging protocol (18) was used to detect and quantify the colocalization of APP and δ-COP simultaneously with a Golgi marker in living N2a cells. We found that GFP-APP and CFP-δ-COP highly colocalize and reside predominantly in the Golgi compartment (Fig. 5 *A*–*C* and Fig. S2). The role of COPI in Golgi-to-ER retrograde trafficking is well established (19), but a role for δ-COP in APP trafficking has not been reported. To investigate the effects of δ-COP–induced retrograde transport on APP dynamic trafficking, we imaged living cells, with or without δ-COP silencing, using inverse fluorescence recovery

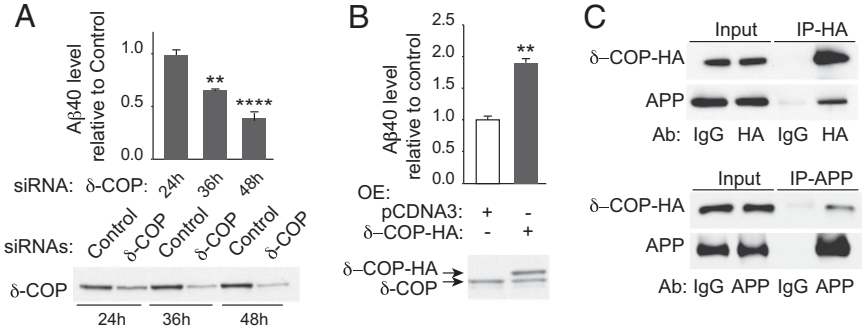

Fig. 2. Effects of δ-COP on Aβ40 production and evaluation of δ-COP/APP interaction. (*A*) Time course analysis of Aβ40 level (*Upper*) in response to inhibition of δ-COP expression (*Lower*). (*B*) Overexpression of δ-COP-HA in N2a-695 cells pretreated with δ-COP siRNAs (*Lower*) and measurement of Aβ40 level (*Upper*). (*C*) Immunoprecipitation (IP) of δ-COP-HA (*Upper*) and APP (*Lower*) (**$P < 0.01$, ****$P < 0.0001$; two-tailed Student's *t* test; $n = 3$).

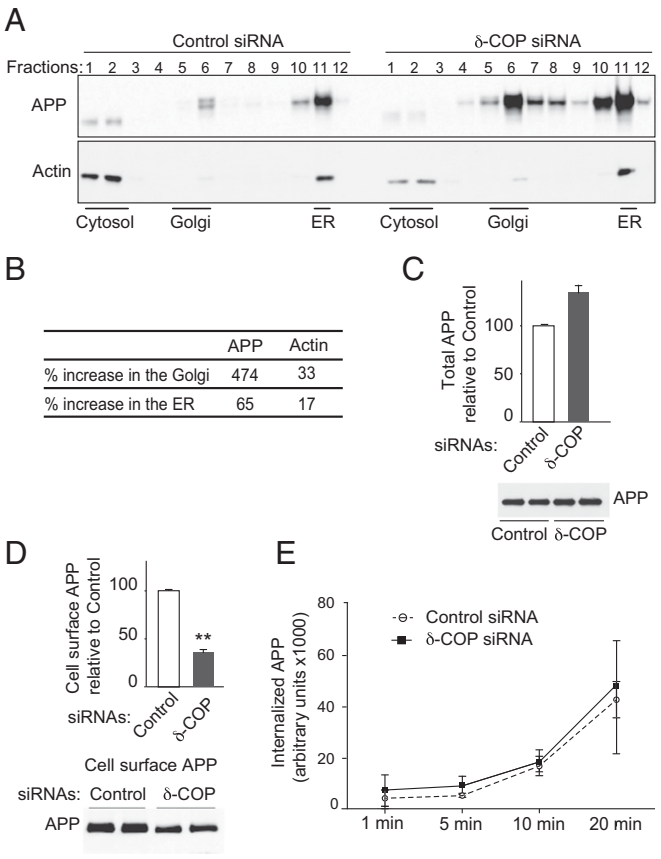

Fig. 3. Effect of δ-COP on APP localization. (*A*) Subcellular localization of APP and actin in N2a-695 cells transfected with control siRNA (*Left*) or δ-COP siRNA (*Right*) by sucrose density gradient fractionation. (*B*) Protein expression was evaluated by Western blotting analysis and quantified 48 h posttransfection with δ-COP siRNA. (*C*) Total APP measurement following transfection with δ-COP siRNA by Western blotting analysis (*Lower*) and quantification (*Upper*). (*D*) Cell surface expression of APP was analyzed by Western blotting analysis (*Lower*) and quantified using cell surface biotinylation (*Upper*). (*E*) Biotinylation experiments were conducted to study APP internalization in N2a-695 cells transfected with δ-COP siRNA. Biotinylated proteins were internalized at 37 °C for different amounts of time (1 min, 5 min, 10 min, and 20 min). The internalized APP was analyzed by Western blotting and quantified (**$P < 0.01$, two-tailed Student's t test; $n = 3$).

after photobleaching (iFRAP). N2a cells, with the exception of the Golgi area, were repeatedly photobleached, and the loss of APP fluorescence in the Golgi apparatus was tracked as GFP-APP exited the Golgi. The treatment with δ-COP siRNA dramatically delayed the loss of fluorescence compared with nonsilenced cells (Fig. 5 *D* and *F*, δ-COP silencing efficiency is shown in Fig. 5*E*), demonstrating that δ-COP is a key regulator of APP Golgi localization. To examine the movement of APP after exiting the Golgi, we coexpressed a photoactivatable APP-GFP (APP-paGFP) and a marker of the Golgi apparatus, mCherry-galactotransferase (GalT-mCherry) with a single plasmid. We tracked the movement of APP by activating the most distal region of the trans-Golgi network to enable recording of the retrograde movement toward the nucleus. Several vesicles that appeared in the control condition (Fig. 6*A*, *Top*, white arrows) moved toward the nucleus over time. However, after silencing δ-COP (Fig. 6*B*), the activated APP remained immobile, demonstrating the necessity of δ-COP for the retrograde transport of APP.

Discussion

Reduction or prevention of Aβ peptide accumulation remains an important goal of AD research and treatment. Along these lines, new clinical trials are aimed at targeting the pathways underlying Aβ production (20, 21). The present results indicate that δ-COP interacts with APP and plays an important role in its processing. Knockdown of δ-COP results in an accumulation of APP in the Golgi, while decreasing its maturation and expression at the plasma membrane. Consequently, it reduces the production of Aβ peptides. The effect of δ-COP on Aβ peptide regulation could be explained by two main hypotheses: (*i*) the interference with the retrograde transport leading indirectly to lower amounts of APP reaching the cell surface and being available for cleavages by the secretases within endocytic compartments and/or (*ii*) reduced APP endocytosis as a consequence of downstream pathway regulation by the COPI complex (22, 23). Here, we demonstrated that the kinetics of APP endocytosis remain mostly unchanged after reducing δ-COP, privileging the former hypothesis.

Furthermore, the data presented from live-cell imaging experiments corroborate this hypothesis clearly, showing that by using state-of-the-art iFRAP technology, less APP is exiting the Golgi after silencing δ-COP and that use of photoactivable APP allowed us to follow dynamically the retrograde transport, further demonstrating the importance of δ-COP for APP Golgi localization.

The correlation between inhibition of APP maturation and APP retention in the Golgi apparatus after δ-COP silencing suggests that a quality-control mechanism prevents APP from moving further in the secretory pathway. Indeed, it is known that if a misfolded protein exits the ER, COPI contributes to its retrieval back to the ER, providing the environment for protein folding (9, 24). Therefore, it is possible that δ-COP impairment affects the quality control of APP and that incorrect APP molecules cannot undergo maturation steps as suggested by the present work. Proteins are transported beyond the Golgi apparatus only if they are fully folded and maturated. For this reason, higher levels of APP in the Golgi apparatus do not necessarily translate into an increased level of APP in downstream compartments, such as the plasma membrane. By reducing or blocking COPI function, we propose that the reduced function prevents full maturation of APP. Along these lines, inhibition of the retrograde trafficking route is thought to lead to the collapse of anterograde trafficking (25). Altogether, these results might explain why COPI loss of function leads to an accumulation of APP not only in the Golgi but also in the ER to a lesser extent.

In contrast to the classical paradigm centered on the proteolytic cleavages of APP to release Aβ, a possible model that takes into account our results would imply that the formation of Aβ might be controlled by the posttranslational state of APP, occurring upstream from the processing sites (endocytic pathway). Changes in APP PTMs, such as the addition of new biochemical moieties (e.g., glycosylation, palmitoylation) could alter both its targeting to downstream cellular compartments and its cleavage by secretases. This result suggests that APP maturation steps need to occur sequentially in the Golgi/ER compartments. The preliminary data suggest that N-glycosylation of APP, known to occur in the ER (15), could be one necessary PTM for the downstream regulation of Aβ production.

It has been shown that TMP21, a protein associated with COPI, is a component of the γ-secretase complex and regulates its activity (26). Interestingly, the γ-secretase complex has been found in COPI-coated vesicles and linked to APP trafficking (12, 27). In the context of AD etiology, these studies and the work that we have presented here highlight a broad regulatory role of retrograde transport. This fact reinforces the importance of early quality-control steps in AD pathogenesis and raises the question of a possible derailment over time.

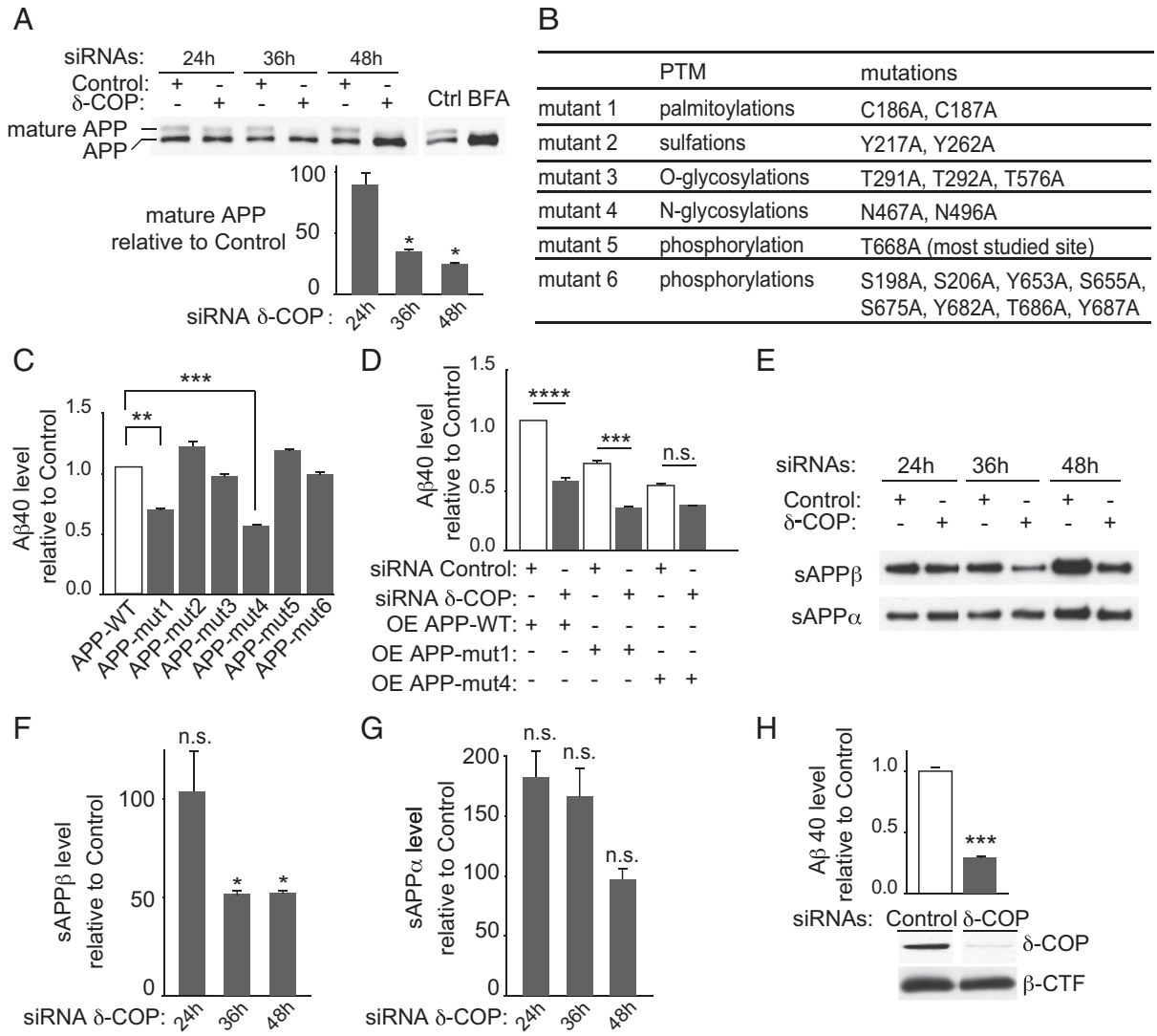

	PTM	mutations
mutant 1	palmitoylations	C186A, C187A
mutant 2	sulfations	Y217A, Y262A
mutant 3	O-glycosylations	T291A, T292A, T576A
mutant 4	N-glycosylations	N467A, N496A
mutant 5	phosphorylation	T668A (most studied site)
mutant 6	phosphorylations	S198A, S206A, Y653A, S655A, S675A, Y682A, T686A, Y687A

Fig. 4. Effect of δ-COP on APP metabolism. (*A*) Maturation of APP after transfection with δ-COP siRNA or BFA treatment (*Upper*) and quantification of mature APP (*Lower*). Ctrl, control. (*B*) Position and nature of the APP mutations engineered. (*C*) Aβ40 level measurements 48 h posttransfection of N2a cells overexpressing APP-WT or the six different APP mutants. (*D*) Overexpression of APP-WT, APP-mut1, or APP-mut4 in N2a cells pretreated with siRNAs (control or δ-COP) and measurement of Aβ40 level. (*E*) Visualization of sAPPbeta and sAPPalpha in N2a-695 cells transfected with δ-COP siRNA. Quantification of sAPPbeta (*F*) and sAPPalpha (*G*). (*H*) γ-Secretase cleavage quantification in N2a cells overexpressing the APP-beta-CTF. δ-COP and APP-beta-CTF expression (*Lower*) and Aβ40 production (*Upper*) are shown (**P* < 0.05, ***P* < 0.01, ****P* < 0.001, *****P* < 0.0001, two-tailed Student's *t* test and Bonferroni's multiple comparison test; *n* = 3). n.s., not significant.

Materials and Methods

Biochemistry.

Cell culture, cell viability, cell death assessments, knockdown, and overexpression. N2a cells overexpressing APP695 (N2a-695) and N2a cells were grown in 1:1 DMEM/Opti-MEM (Life Technologies) containing 5% (vol/vol) FBS (Sigma). HEK 293T cells were grown in DMEM supplemented with 10% (vol/vol) FBS. For cellular knockdown experiments, siRNA of the COPI subunits was purchased from Thermo Fisher Scientific. The siRNAs used were purchased as a pool of four different siRNAs. For δ-COP, we also used an individual siRNA sequence. N2a-695 and N2a cells were transfected with siRNA using DharmaFect 2 (Thermo Fisher Scientific). Nontargeting control siRNA (Thermo Fisher Scientific) was transfected in parallel as a control. For overexpression in cells, mammalian expression vector pReceiver-M07 coding different proteins with a C-terminal HA tag was purchased from Genecopoeia. Plasmids were transfected into cells using Lipofectamine 2000 (Life Technologies). The pcDNA4-beta-CTF expression vector was a kind gift from Y. M. Li (Memorial Sloan Kettering Cancer Center, New York). PcDNA3-APP was provided by H. Rebholz, The City College of New York, New York. BFA (Sigma), a drug known to disrupt the Golgi apparatus physically, was used as a control. APP mutant sites for the PTM studies were chosen based on the existing literature and were designed following standard procedures. A cytotoxicity kit was purchased from Promega. Cell death was determined by measuring the level of lactate dehydrogenase activity released upon cell lysis.

Aβ quantification. For cell cultures, the medium was replaced 6 h before collecting supernatants for Aβ40 and Aβ42 peptide measurements. Aβ levels were normalized to total protein levels. The concentrations of Aβ40 peptide were determined using the sandwich ELISA technique (Life Technologies).

Western blotting analysis and Abs. Equal amounts of protein samples (based on bicinchoninic acid assay quantification) were subjected to Western blot analysis. Abs used were as follows: APP-CTF (in-house and Abcam), APP (6E10 from Covance), δ-COP, (Abcam), β-actin (EMD Millipore), PS1 (in-house), and Myc (Genscript). HA Ab for immunoprecipitation (Genscript) and HA Ab for Western blotting (Roche) were also used.

Real-time RT-PCR. RNAs were extracted from cells using a PureLink RNA Extraction Mini Kit (Life Technologies). Equal amounts of RNA were used to set up RT-PCR to generate cDNAs using a High Capacity cDNA Reverse Transcription Kit (Life Technologies). cDNAs were used for real-time PCR using Taqman Gene Expression Assays (Life Technologies).

Coimmunoprecipitation. HEK 293T cells overexpressing δ-COP–HA were lysed in 50 mM Hepes, 150 mM NaCl, 1% CHAPSO (3-([3-Cholamidopropyl]dimethylammonio)-2-hydroxy-1-propanesulfonate), 5 mM $MgCl_2$, and 5 mM $CaCl_2$, with protease inhibitors. Immunoprecipitation experiments were performed using the

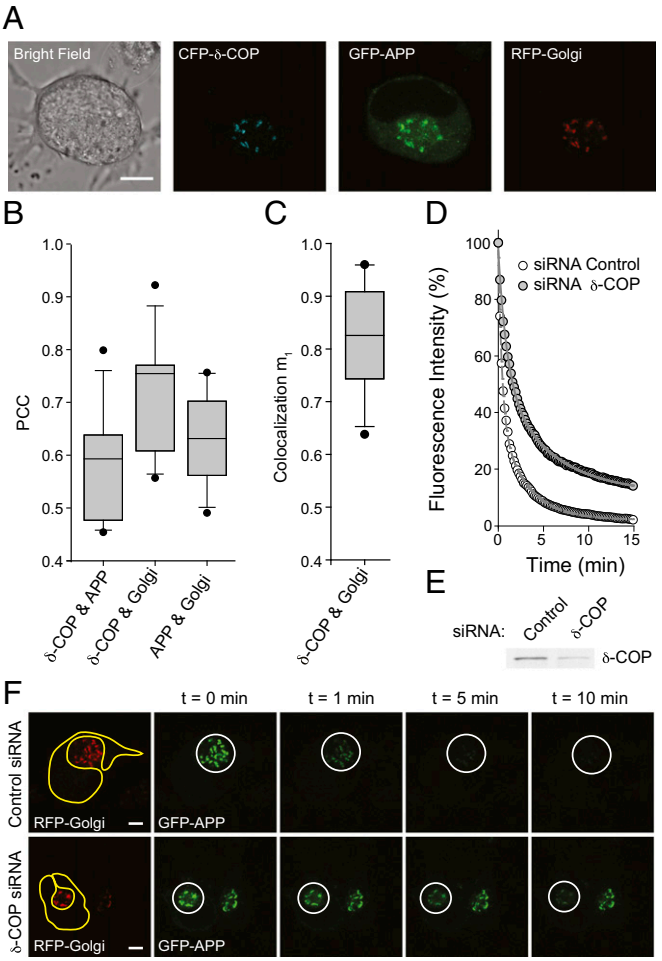

Fig. 5. Influence of δ-COP on APP trafficking in living cells. (*A*) Subcellular localization of APP, Golgi, and δ-COP in living N2a cells infected with a baculovirus expressing an RFP-Golgi marker, and then transfected with CFP-δ-COP and GFP-APP ($n = 3$). (Scale bar: 10 μm.) (*B*) Box plot of Pearson's correlation coefficient (PCC). Values for each of the three conditions are greater than 0.5, indicating positive colocalization for each duo considered. (*C*) Colocalization coefficients m1 plot for CFP-δ-COP and RFP-Golgi ($n = 12$). (*D*) Time-course quantification of iFRAP kinetics ($n = 6$–10 cells from independent culture dishes). (*E*) δ-COP expression in N2a cells used for the iFRAP live-cell imaging ($n = 3$). (*F*) Images from iFRAP time series of GFP-APP (*Right*) under repeated photobleaching of single cells excluding the Golgi region (*Left*). The bleached area is highlighted in yellow, and the region of interest for measuring fluorescence loss is circled in white. (*Lower*) Two cells are visible on the field under δ-COP siRNA treatment, but iFRAP was performed on only one of them. (Scale bar: 10 μm.)

appropriate Abs mixed with Protein G Plus/Protein A Agarose beads (EMD Millipore) and incubated for 2 h at 4 °C. The samples were washed with lysis buffer, and proteins were eluted with SDS loading buffer. Immunoprecipitated proteins were resolved by SDS/PAGE and analyzed by Western blot using appropriate Abs.

Subcellular fractionation. Cells were homogenized in a sucrose buffer [0.25 M sucrose, 10 mM Tris (pH 7.4), 2 mM MgAc, 0.5 mM EDTA supplemented with protease inhibitors] using a ball-bearing cell cracker. Homogenates were loaded on top of a step sucrose gradient [10 mM Tris (pH 7.4), 1 mM MgAc, 0.25–2 M sucrose]. The gradients were centrifuged for 2.5 h at 250,000 × *g* using a Beckman SW41Ti rotor. Twelve 1-mL fractions were collected and analyzed by SDS/PAGE and Western blotting using APP-CTF Ab (discussed above). Fractions corresponding to the Golgi and ER specifically were also analyzed by SDS/PAGE and Western blotting using corresponding antibodies for APP-CTF and actin (discussed above).

Cell surface biotinylation. Cells were washed with ice-cold PBS and incubated with Sulfo-NHS-SS-Biotin (Thermo Fisher Scientific) in PBS for 30 min at 4 °C. Biotin solution was then removed, and cells were washed once with 50 mM Tris and twice with ice-cold PBS.

Biotin assay for endocytosis. Cells were washed with ice-cold PBS/CM (PBS containing 1 mM $MgCl_2$ and 1.3 mM $Cacl_2$) and incubated with Sulfo-NHS-SS-Biotin in PBS/CM. Biotin solution was then removed, and cells were washed twice with DMEM/0.2% BSA (Life Technologies and Jackson ImmunoResearch Laboratories). Cells were transferred to 37 °C for various times to allow the biotinylated proteins to be internalized. The reactions were stopped by transferring the cells and washing twice in PBS/CM containing 10% serum at 4 °C (Life Technologies). The cells were incubated in reducing solution and then quenching solution.

Precipitation of biotinylated proteins. Cells were collected and lysed in radioimmunoprecipitation assay buffer, followed by centrifugation. Lysates were added to streptavidin-Dynabeads (Life Technologies) and incubated for 1 h at 4 °C. The beads were then washed five times with ice-cold PBS/0.01% Tween and eluted by addition of SDS loading buffer. Biotinylated proteins were resolved by SDS/PAGE and analyzed by Western blot with APP Ab.

Live-Cell Imaging and Analysis.

Cell culture. N2a cells were cultured on poly-D-lysine–coated, glass-bottomed culture dishes (MatTek Corp). Cells were initially maintained in 1:1 DMEM/Opti-MEM (Life Technologies) containing 5% FBS for 24 h. Neurite differentiation was induced by reducing serum in the medium (1% FBS) for another 48 h. Golgi localization was achieved by infection with a baculovirus to express CellLight RFP-Golgi marker (Life Technologies). CFP-δ-COP and GFP-APP were transfected into N2a cells using Lipofectamine 2000. For iFRAP experiments, an additional siRNA treatment procedure was performed 6 h before the transfection step.

Live-cell confocal microscopy. All images were acquired 24–30 h after transfection. Live-cell confocal images were obtained on a Leica TCS SP8 confocal imaging system equipped with 63×/1.4 and 100×/1.4 N.A. oil-immersion objective lenses. During imaging, cells were maintained in 1:1 DMEM/Opti-MEM without Phenol Red on a stage preheated to 37 °C. Microscopy setup and imaging acquisition were performed as described previously (28). A white-light laser source (Leica WLL) providing a continuous spectral output between 470 and 670 nm and a 405-nm UV laser was used for excitation. The microscope was maintained at 32–35 °C using a temperature-controlled housing throughout the entire imaging procedures.

Statistical analyses for colocalization. Twelve sets of micrographs from three independent experiments were used for colocalization analysis. The Pearson's correlation coefficient (PCC) was determined using Image-Pro Premier (version 9.1; Media Cybernetics) as described previously (18). To measure the fraction of total CFP-δ-COP fluorescence (denoted as *C*) that colocalized with the RFP-Golgi fluorescence (denoted as *R*), we further calculated Manders' colocalization coefficients (m_1) using Image-Pro Premier based on the equation below (*Ch*, channel; *i*, intensity):

$$m_1 = \frac{\sum_i Ch(C)_{i,coloc\ (C\&R)}}{\sum_i Ch(C)_i}.$$

iFRAP imaging and analysis. A Zeiss LSM 780 laser-scanning confocal microscope equipped with a 100×/1.4 N.A. oil-immersion objective lens and a 25-mW multiline argon laser was used for all iFRAP imaging. Selective photobleaching was performed repeatedly at 30% laser power before each time-lapse image was taken. Each photobleaching iteration took 5–8 s depending on the size of bleached areas. Total time-lapse scanning was set at 80–120 scans (15 min) with 5 s between scans. Three prescans were performed to establish the baseline. Fluorescent quantitation was performed using ZEN microscope software (Carl Zeiss Microscopy), where the mean intensities of the GFP-APP in the Golgi region were measured. Apparent fluorescent decrease was fitted using a single exponential function: $I_{(t)} = I_\infty + I_0 \times e^{-(t/T)}$, where I_∞ is the final remaining fluorescence at the end of the time series, I_0 is the initial fluorescence, and T is the apparent decay time constant. A collection of six to 10 independent experimental datasets was used for calculation and plotted using SigmaPlot (version 11.0; Systat Software). Fluorescence decrease was plotted as a function of time and fitted to a single exponential (Fig. 5*D*).

Photoactivation experiments. Confocal microscope setup for live-cell imaging of paGFP was performed as described previously (29). The pa-GFP plasmid was a generous gift from George Patterson, National Institute of Biomedical Imaging, Bethesda. In brief, N2a cells were transfected with a custom-designed plasmid (pBudCE4.1 backbone expression vector; Life Technologies) that simultaneously expresses APP-paGFP and GalT-mCherry. GalT-mCherry–expressing cells were selected for photoactivation. Cultured cells were kept on a heated stage connected to temperature and CO_2 control units (PeCon GmbH). The Zeiss photobleaching mode was used to photoactivate paGFP. Localized photoactivation of APP-paGFP on a region of the trans-Golgi network furthest from the nucleus, which was marked by GalT-mCherry fluorescence (a marker of the Golgi apparatus), was triggered with acousto-optic tunable filters switched 405-nm solid-state laser. Time-lapse live-cell imaging

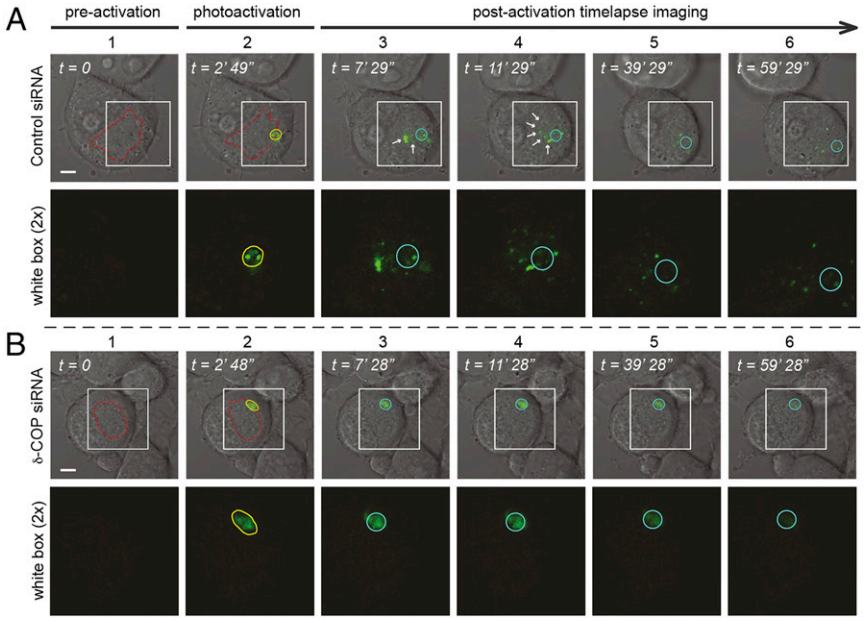

Fig. 6. Effect of δ-COP on retrograde movement in living cells. Single N2a cells expressing APP-paGFP treated with control siRNA (*A*) or δ-COP siRNA (*B*) and subjected to photoactivation (column 2). Time-lapse images of APP-paGFP (columns 3–6). Fluorescent signals are merged with bright-field images, and the region of interest highlighted with a white box is shown under each field. (Magnification: 2×.) The morphology of the plasma membrane and nucleus of the cells were visualized by differential interference contrast (DIC) microscopy. Regions of the Golgi are outlined in red using the expression of GalT-mCherry. Yellow circles in the second column indicate the photoactivated region (trans-Golgi). Light blue circles in the third to sixth columns mark the photoactivated regions, and white arrows show the movement of APP over time ($n = 3$). (Scale bars: 10 μm.)

was resumed immediately following photoactivation, and 100 imaging frames were taken in 1 h. The confocal scanning rate was set at 3.15 μs per pixel with line average up to 2, which translates to acquisition speeds ranging from 1 to 2 s per image. Both static and dynamic movies were annotated and edited for presentation using Zeiss Zen 2012 software.

ACKNOWLEDGMENTS. We thank Dr. Jean-Pierre Roussarie for his critical reading of the manuscript. We thank Dr. George Patterson for the paGFP clone. This work was supported, in part, by grants from the US NIH (National Institute on Aging Grant AG-09464 to P.G.), Fisher Center for Alzheimer's Research Foundation (to P.G. and M.F.), and Cure Alzheimer's Fund (to P.G.).

1. Haass C, Kaether C, Thinakaran G, Sisodia S (2012) Trafficking and proteolytic processing of APP. *Cold Spring Harb Perspect Med* 2(5):a006270.
2. Swerdlow RH, Burns JM, Khan SM (2010) The Alzheimer's disease mitochondrial cascade hypothesis. *J Alzheimers Dis* 20(Suppl 2):S265–S279.
3. Nixon RA, Yang DS (2011) Autophagy failure in Alzheimer's disease–locating the primary defect. *Neurobiol Dis* 43(1):38–45.
4. Thinakaran G, Koo EH (2008) Amyloid precursor protein trafficking, processing, and function. *J Biol Chem* 283(44):29615–29619.
5. Griciuc A, et al. (2013) Alzheimer's disease risk gene CD33 inhibits microglial uptake of amyloid beta. *Neuron* 78(4):631–643.
6. Vassar R, Kovacs DM, Yan R, Wong PC (2009) The beta-secretase enzyme BACE in health and Alzheimer's disease: Regulation, cell biology, function, and therapeutic potential. *J Neurosci* 29(41):12787–12794.
7. Wolfe MS (2008) Gamma-secretase: Structure, function, and modulation for Alzheimer's disease. *Curr Top Med Chem* 8(1):2–8.
8. Choy RW, Cheng Z, Schekman R (2012) Amyloid precursor protein (APP) traffics from the cell surface via endosomes for amyloid β (Aβ) production in the trans-Golgi network. *Proc Natl Acad Sci USA* 109(30):E2077–E2082.
9. Beck R, Rawet M, Wieland FT, Cassel D (2009) The COPI system: Molecular mechanisms and function. *FEBS Lett* 583(17):2701–2709.
10. Lee MC, Miller EA, Goldberg J, Orci L, Schekman R (2004) Bi-directional protein transport between the ER and Golgi. *Annu Rev Cell Dev Biol* 20:87–123.
11. Rabouille C, Klumperman J (2005) Opinion: The maturing role of COPI vesicles in intra-Golgi transport. *Nat Rev Mol Cell Biol* 6(10):812–817.
12. Selivanova A, Winblad B, Farmery MR, Dantuma NP, Ankarcrona M (2006) COPI-mediated retrograde transport is required for efficient gamma-secretase cleavage of the amyloid precursor protein. *Biochem Biophys Res Commun* 350(1):220–226.
13. Bhattacharyya R, Barren C, Kovacs DM (2013) Palmitoylation of amyloid precursor protein regulates amyloidogenic processing in lipid rafts. *J Neurosci* 33(27):11169–11183.
14. Walter J, Haass C (2000) Posttranslational modifications of amyloid precursor protein: Ectodomain phosphorylation and sulfation. *Methods Mol Med* 32:149–168.
15. Schedin-Weiss S, Winblad B, Tjernberg LO (2014) The role of protein glycosylation in Alzheimer disease. *FEBS J* 281(1):46–62.
16. Oishi M, et al. (1997) The cytoplasmic domain of Alzheimer's amyloid precursor protein is phosphorylated at Thr654, Ser655, and Thr668 in adult rat brain and cultured cells. *Mol Med* 3(2):111–123.
17. Barbagallo AP, et al. (2010) Tyr(682) in the intracellular domain of APP regulates amyloidogenic APP processing in vivo. *PLoS One* 5(11):e15503.
18. Tian Y, Chang JC, Fan EY, Flajolet M, Greengard P (2013) Adaptor complex AP2/PICALM, through interaction with LC3, targets Alzheimer's APP-CTF for terminal degradation via autophagy. *Proc Natl Acad Sci USA* 110(42):17071–17076.
19. Lippincott-Schwartz J, Liu W (2006) Insights into COPI coat assembly and function in living cells. *Trends Cell Biol* 16(10):e1–e4.
20. Mills SM, et al. (2013) Preclinical trials in autosomal dominant AD: Implementation of the DIAN-TU trial. *Rev Neurol (Paris)* 169(10):737–743.
21. Moulder KL, et al. (2013) Dominantly Inherited Alzheimer Network: facilitating research and clinical trials. *Alzheimers Res Ther* 5(5):48.
22. Whitney JA, Gomez M, Sheff D, Kreis TE, Mellman I (1995) Cytoplasmic coat proteins involved in endosome function. *Cell* 83(5):703–713.
23. Styers ML, O'Connor AK, Grabski R, Cormet-Boyaka E, Sztul E (2008) Depletion of beta-COP reveals a role for COP-I in compartmentalization of secretory compartments and in biosynthetic transport of caveolin-1. *Am J Physiol Cell Physiol* 294(6):C1485–C1498.
24. Yamamoto K, et al. (2001) The KDEL receptor mediates a retrieval mechanism that contributes to quality control at the endoplasmic reticulum. *EMBO J* 20(12):3082–3091.
25. Brandizzi F, Barlowe C (2013) Organization of the ER-Golgi interface for membrane traffic control. *Nat Rev Mol Cell Biol* 14(6):382–392.
26. Chen F, et al. (2006) TMP21 is a presenilin complex component that modulates gamma-secretase but not epsilon-secretase activity. *Nature* 440(7088):1208–1212.
27. Réchards M, et al. (2006) Presenilin-1-mediated retention of APP derivatives in early biosynthetic compartments. *Traffic* 7(3):354–364.
28. Chang JC, et al. (2012) Single molecule analysis of serotonin transporter regulation using antagonist-conjugated quantum dots reveals restricted, p38 MAPK-dependent mobilization underlying uptake activation. *J Neurosci* 32(26):8919–8929.
29. Patterson GH, Lippincott-Schwartz J (2002) A photoactivatable GFP for selective photolabeling of proteins and cells. *Science* 297(5588):1873–1877.